2016

An Integrated Model for an Oil Free Carbon Dioxide Compressor Using Sanderson-Rocker Arm Motion Mechanism

Bin Yang
Purdue University, United States of America, yang62@purdue.edu

Orkan Kurtulus
Purdue University, United States of America, orkan@purdue.edu

Eckhard Groll
Purdue University, United States of America, groll@purdue.edu

An Integrated Model for an Oil Free Carbon Dioxide Compressor Using Sanderson-Rocker Arm Motion (S-RAM) Mechanism

Bin YANG[1*], Orkan KURTULUS[2], and Eckhard A. GROLL[3]

Purdue University, School of Mechanical Engineering,
Ray W. Herrick Laboratories, West Lafayette, IN, USA

[1]yang62@purdue.edu
[2]orkan@purdue.edu
[3]groll@purdue.edu

* Corresponding Author

ABSTRACT

The multi-piston axial reciprocating compressor using the Sanderson-Rocker Arm Motion (S-RAM) mechanism is expected to have high volumetric efficiencies due to the application of a new type of seal to prevent the in-cylinder refrigeration gas leaking through the clearance between piston and cylinder wall. The stroke of the compressor can be controlled by adjusting the inclination angle between the connecting shaft and machine driving shaft. This allows the control of the delivered refrigerant mass flow rate to match the capacity requirement in the field.

A comprehensive simulation model to predict the performance of a prototype reciprocating compressor using the S-RAM mechanism has been developed. The natural refrigerant carbon dioxide (CO_2) is used as the working fluid. The comprehensive model is comprised of a kinematics model, compression process model and an overall energy balance model. In the kinematics model, the movement of the piston is given including its displacement, velocity and acceleration. It is found that the moving path of the center of the ball in the ball-socket joint is moving around a corresponding cylinder centerline with a 'figure 8' motion instead of moving along the cylinder centerline. In the compression process model, the system of governing equations is solved, which incorporates a valve sub-model, leakage sub-model and gas pulsation sub-model. The classical 4th order Runge-Kutta method and Broyden's method are employed to solve the non-linear system of equations to find the in-cylinder refrigerant state (temperature, pressure) at each rotational angle of the machine driving shaft. The variations of suction and discharge valve movements with respect to drive shaft rotational angle are also given. The values of the cylinder wall temperature, the actual suction and discharge temperatures in the connecting pipes are required to initiate the solving of the compression process model. These temperatures are solved simultaneously by incorporating the overall energy balance model with the compression process model. A lumped temperature assumption is employed in the overall energy balance model to assume there is no temperature gradient in each compressor component at steady-state.

1. INTRODUCTION

Since Lorentzen and Pettersen presented experimental data on an automotive air conditioning system using CO_2 as the refrigerant in early the 90's last century (1992), tremendous research activities have been carried out on the application of CO_2 as an alternative refrigerant in refrigeration systems. Some of the activities were dedicated to the development of a CO_2 reciprocating compressor. Fagerli (1997) theoretically and experimentally investigated the possibility of the application of small hermetic reciprocating compressors in the CO_2 trans-critical cycle. The prototype single cylinder CO_2 compressor was retrofitted from an existing compressor using R22 as the working fluid. It was shown that the overall isentropic efficiency of the CO_2 compressor was lower than R22 compressor by 9% to 15%, the volumetric efficiency was lower by 5%. Süss and Kruse (1998) proposed that it was possible for a CO_2 compressor to achieve a higher performance by an appropriate design, since the pressure ratio was lower

compared to that in a compressor using conventional refrigerant as the working fluid. Nekså et al. (1999) developed a series of semi-hermetic reciprocating compressors using CO_2 as the working fluid whose displacements expanded from 1.7 $m^3 \cdot h^{-1}$ to 10.7 $m^3 \cdot h^{-1}$. These compressors were single- or double-cylinders. It was shown in the experiments that the single-cylinder compressors could reach an overall isentropic efficiency of 0.69 and a volumetric efficiency of 0.77 if used in a water heating heat pump. Bauman and Conzett (2002) developed a non-lubricated four-cylinder prototype reciprocating compressor. Experiments showed an acceptable efficiency. By now, several commercial company mass produced single- and double-cylinder semi-hermetic reciprocating compressors used in trans-critical CO_2 systems (2015).

Meanwhile, simulation models were also developed to reveal the distinct characteristics of a reciprocating compressor using CO_2 as its working fluid. Yang et al. (2013) developed a comprehensive simulation model for a semi-hermetic two-cylinder reciprocating compressor. In this model, both the frictional power losses between piston rings and cylinder wall and that at the bearings were calculated. The simulation results were in a good agreement with the compressor performance measurements. Cavalcante et al. (2008) developed a transient model for a CO_2 automotive swash plate compressor in which the piston moved with a reciprocating motion. The in-cylinder thermodynamic phenomenon, valve dynamics, heat transfer, friction of swash plate and pistons, leakage through pistons were taken into account

The work presented in this paper focuses on a comprehensive simulation model for a novel prototype reciprocating compressor using the Sanderson-Rocker Arm Motion (S-RAM) driving mechanism, which converts the rotation of machine driving shaft into a reciprocating motion of a piston at high efficiency. The S-RAM compressor is expected to be promising in heat pump and cooling applications of 25 to 300 kW capacities. It has competitive volumetric efficiencies and overall isentropic efficiencies compared to other types of compressors used in this range of cooling capacities, such as scroll compressors and screw compressors. The schematic of the S-RAM mechanism can be seen in Figure 1. The machine driving shaft is coupled with an AC motor shaft. One end of the inclined shaft is fixed in a shoe. The other end of the connecting shaft forms conjunction with another shaft through a universal joint. The position of the universal joint is fixed relative to machine driving shaft when the compressor is running. The inclined angle between the connecting shaft and machine driving shaft keeps constant when the compressor is spinning. The wobble plate makes a nutation around the universal joint. There are five ball-socket joints connected the wobble plate and piston assembly. The centers of these balls form a wobble plane which goes through the universal joint. The ball-socket joint converts the rotation of machine driving shaft into a reciprocating motion of pistons.

There are several advantages using the S-RAM mechanism. First, the capacity of compressor can be changed by changing the stroke without varying the motor speed. This can be achieved by changing the inclined angle of the connecting shaft to the machine driving shaft. While the stroke is varying, the position of the top dead center (T.D.C.) relative to the machine itself is fixed, i.e., the clearance volume above the piston keeps constant which is one of the main advantages of this compressor. Second, the piston is strictly moving along the cylinder centerline, i.e., there is no side loads resulted from the contact between piston and cylinder wall, reducing the frictional power loss. Finally, a U-cup seal is employed instead of conventional piston rings to prevent the gas from leaking out of the in-cylinder control volume.

2. SIMULATION MODEL OF THE S-RAM COMPRESSOR

2.1 Geometric and kinematics model

Figure 1 shows a schematic of the driving system of the Sanderson-Rocker Arm Motion mechanism. A coordinate system is built to assist the establishment of the kinematics model. The $X_0Y_0Z_0$ coordinate system is located on the machine itself. The XYZ coordinate system is obtained by rotating $X_0Y_0Z_0$ counterclockwise (seen from up direction) around the Z_0-direction by a degree of θ. Rotating the XYZ coordinate system around the X-direction counterclockwise by a degree of α, forms the X'Y'Z' coordinate system, which is located on the wobble plane. The wobble plane is formed by the moving path of the ball centers. The three coordinate systems have the same origin, which is located at the center of the universal joint.

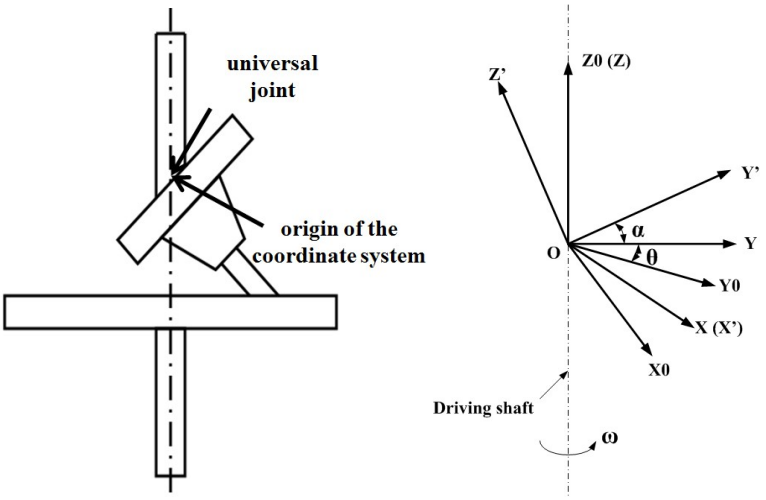

Figure 1: Coordinate system used in kinematics model

Through the transformation of the coordinate systems, the *i*-th ball center position in the XYZ system can be shown as

$$\begin{cases} X = R_w \cos(-\theta' + \theta_i) \\ Y = R_w \sin(-\theta' + \theta_i)\cos\alpha \\ Z = R_w \sin(-\theta' + \theta_i)\sin\alpha \end{cases}. \quad (1)$$

Where, R_w is the radius of the wobble plate. θ' is the rotational angle of *i-th* ball center in X'Y'Z' coordinate system. θ_i is the *i*-th cylinder phase angle. α is the wobble plate tilting angle. The position of the *i*-th ball center in $X_0Y_0Z_0$ system is then determined using the following equations,

$$\begin{cases} X_0 = R_w \cos(-\theta' + \theta_i)\cos\theta - R_w \sin(-\theta' + \theta_i)\cos\alpha\sin\theta \\ Y_0 = R_w \cos(-\theta' + \theta_i)\sin\theta + R_w \sin(-\theta' + \theta_i)\cos\alpha\cos\theta \\ Z_0 = R_w \sin(-\theta' + \theta_i)\sin\alpha \end{cases}. \quad (2)$$

The piston displacement is calculated using the third equation in Eq. (2). The mid-stroke point is designated as the starting point of the displacement. For convenience, the starting point can be specified to the bottom dead center (B.D.C.) or the top dead center (T.D.C.) by shifting calculated values correspondingly. The direction towards to the T.D.C. is assumed to be positive. The piston velocity and acceleration can be determined by further differentiation of Z_0 equation in Eq. (2).

2.2 Compression process model

2.2.1 Governing equations

The thermal properties of the refrigerant inside the cylinder are assumed to be uniform anywhere in the cylinder. According to the law of continuity, the mass change of refrigerant in the cylinder can be expressed by:

$$\frac{dm_c}{dt} = \frac{dm_{suc}}{dt} + \frac{dm_{li}}{dt} - \frac{dm_{dis}}{dt} - \frac{dm_{lo}}{dt}. \quad (3)$$

Where, m_c refers to the refrigerant mass in the cylinder.

The energy conservation equation can be derived by applying the first law of thermodynamics to the in-cylinder control volume:

$$\frac{dT_c}{dt} = \frac{1}{m_c C_v}[(h_{suc} - h_c)\frac{dm_{suc}}{dt} + (h_{li} - h_c)\frac{dm_{li}}{dt}] + \frac{1}{m_c C_v}\{[-pm_c - T(\frac{\partial p}{\partial T})_v + p]\frac{dv_c}{dt} + \frac{dQ}{dt}\}. \quad (4)$$

The in-cylinder refrigerant pressure in the above quation is determined by temperature T_c and specific volume v_c. The variation of specific volume with respect to time is evaluated by incorporating the kinematics model.

The instantaneous heat transfer between the refrigerant and the cylinder wall is determined using the heat transfer coefficient, proposed by by Todescat et al. (1992). The heat transfer coefficient is defined as follows:

$$h_{heat} = 3 \cdot 0.7 \cdot \frac{\tau_c}{D_p} \left(\frac{\rho_c U_{mean} D_p}{\mu_c}\right)^{0.7} . \tag{5}$$

Then, the heat transfer rate between refrigerant and cylinder wall is calculated:

$$\dot{Q}_{heat} = \frac{dQ}{dt} = h_{heat} A_{heat} (T_c - T_{wall}) . \tag{6}$$

Where, the cylinder wall temperature, T_{wall}, can be assumed to be constant (Adair et al., 1972).

2.2.2 Valve submodel

The mass flow rates through the valves are determined by assuming an isentropic, compressible flow:

$$\dot{m}_{valve} = \frac{dm_{valve}}{dt} = C_{valve} A_{valve} (2\rho_{high} p_{high})^{\frac{1}{2}} \left\{\frac{\kappa}{\kappa - 1}\left[\left(\frac{p_{low}}{p_{high}}\right)^{\frac{2}{\kappa}} - \left(\frac{p_{low}}{p_{high}}\right)^{\frac{\kappa+1}{\kappa}}\right]\right\}^{\frac{1}{2}} . \tag{7}$$

A discharge coefficient C_{valve} of 0.58 is used for the suction valve and a coefficient of 0.6 is used for the discharge valve (Lin and Sun, 2006). A_{valve} denotes the valve opening area for the suction and discharge valves. It can be determined by considering that there are two dominant regions, pressure dominant region and mass flux dominant region. Correspondingly, the motion of the valve plate which is modeled as a one degree-of-freedom problem can be expressed by the following equations (Kim and Groll, 2007),

In pressure dominant region:

$$m_{equivalent} \ddot{x} + k_{spring} x = (p_{high} - p_{low}) A_{vp} + \frac{1}{2} C_D \rho_{port} V_{port}^2 A_{vp} . \tag{8}$$

In mass flux dominant region:

$$m_{equivalent} \ddot{x} + k_{spring} x = \rho_{port} (V_{port} - x) A_{port} + \frac{1}{2} C_D \rho_{port} V_{port}^2 A_{vp} . \tag{9}$$

Where, $m_{equivalent}$ is the equivalent mass of the valve plate spring; k_{spring} is the spring stiffness; C_D is the drag coefficient, which is assumed to be 1.17; and A_{vp} is the area of valve plate.

2.2.3 Leakage submodel

Any gas leaking through the clearance between piston and cylinder wall is modeled as an isentropic, compressible fluid flowing through an orifice. The mass flow rate of the gas leakage is calculated by:

$$\begin{cases} \dot{m}_{gap} = \dfrac{dm_{gap}}{dt} = C_{gap} A_{gap} p_u \left(\dfrac{2}{ZRT_u}\right)^{\frac{1}{2}} \left\{\dfrac{\kappa}{\kappa - 1}\left[\left(\dfrac{p_d}{p_u}\right)^{\frac{2}{\kappa}} - \left(\dfrac{p_d}{p_u}\right)^{\frac{\kappa+1}{\kappa}}\right]\right\}^{\frac{1}{2}}, \dfrac{p_d}{p_u} > 0.54 \\ \dot{m}_{gap} = \dfrac{dm_{gap}}{dt} = C_{gap} A_{gap} p_u \left(\dfrac{\kappa}{ZRT_u}\right)^{\frac{1}{2}} \left[\left(\dfrac{2}{\kappa+1}\right)^{\frac{\kappa+1}{\kappa-1}}\right]^{\frac{1}{2}}, \dfrac{p_d}{p_u} \le 0.54, choked \end{cases} . \tag{10}$$

Where the discharge coefficient C_{gap} is assumed to be 0.86 (Furuhama and Tada, 1961) and the compressible factor Z is determined by using REFPROP (Lemmon, 2012).

2.3 Gas pulsation model in the discharge pipes

When using a reciprocating compressor with multiple cylinders, gas pulsation is an inevitable issue. The gas pulsations in the discharge pipeline are closely related to the motion of the discharge valves. Moreover, they also

depend on the distributed angle of the multiple cylinders. Elson and Soedel (1974) proposed a mathematical steady state model to investigate the gas pulsation in the discharge plenum and the response of the discharge valve by coupling a steady state solution for the acoustic impedance at the valve with the non-linear valve model. It is not necessary to simultaneously solve a number of equations as the classical method (Brablik, 1972) does if the proposed steady state method is used, making it more flexible to a complicated discharge system. In addition, the classical method makes an assumption that the oscillated back pressure in the piping does not affect the flow through the valve which is not a very good description of the real world. Therefore, the steady state method proposed by Elson and Soedel (1974) is employed.

The anechoic assumption is applied. It is assumed that the acoustic wave in the pipeline is a plane wave. Thus, the acoustic impedance at the valve is given as,

$$Z_{imp} = \frac{p_{pul}}{u_{pul}} = \rho_0 c \,. \tag{11}$$

Where, p_{pul} is the oscillated the acoustic pressure in the discharge pipeline. U_{pul} is the gas velocity at the valve. P_0 is the refrigerant gas density in the pipeline and c is the speed of sound.

The gas velocity at the valve is determined first from the compression process model which incorporates the dynamic valve model. Using Eq. (11), the acoustic pressure is found. The actual pressure in the discharge pipeline should be the sum of the determined acoustic pressure and nominal discharge pressure. With the updated discharge pressure, the compression process model is solved again which results in a different gas velocity at the valve, then repeat this procedure until all the parameters are converged.

2.4 Overall energy balance model

In the abovementioned compression process model, the cylinder wall temperature is essential to calculate the heat transfer between refrigerant gas and cylinder wall. In addition, the suction gas temperature and discharge gas temperature are required in the valve model to accurately calculate the mass flow rate across the suction and discharge valves. Besides, the discharge temperature is also used to calculate the characteristic impedance of the gas after the discharge valve in the discharge gas pulsation model. However, all of these three temperatures (cylinder wall temperature, suction/discharge gas temperature) are undetermined. Hence, in this section, the overall energy balance of the compressor is incorporated into the compression process model to find these three temperatures and solve the compression process model simultaneously. Figure 2 shows the overall energy balance of the compressor.

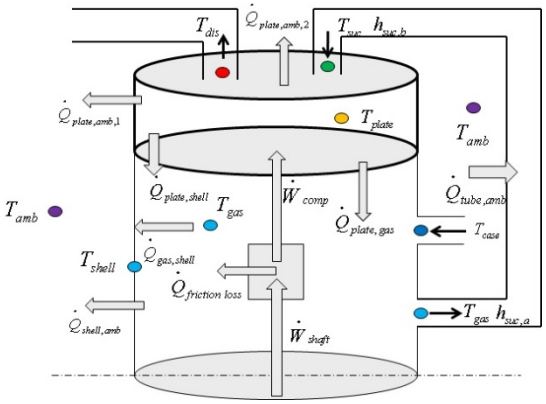

(a)

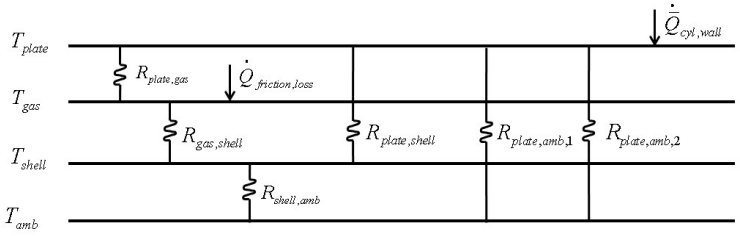

(b)

Figure 2: Energy balance of the compressor

A lumped temperature analysis method is used. There are 5 unknown temperatures: T_{amb}, ,T_{gas}, T_{plate}, T_{suc} and T_{dis}. It is noted here that the cylinder wall temperature is equal to the plate temperature since a lumped temperature analysis method is employed. Applying the energy conservation law to each component, the following equations can be derived:

$$\begin{aligned}
&\dot{m}_{comp}(h_{suc,a}-h_{case})=\dot{Q}_{plate,gas}-\dot{Q}_{gas,shell}+\dot{Q}_{friction,loss}\\
&\dot{Q}_{gas,shell}-\dot{Q}_{shell,amb}=0\\
&-\dot{Q}_{plate,amb,1}-\dot{Q}_{plate,amb,2}-\dot{Q}_{plate,gas}-\dot{\bar{Q}}_{cyl,wall}=0\\
&\dot{Q}_{pipe,amb}+\dot{m}_{comp}(h_{suc,a}-h_{suc,b})=0\\
&\dot{W}_{comp}+\dot{\bar{Q}}_{cyl,wall}=\dot{m}_{comp}(h_{dis}-h_{suc,b})
\end{aligned} \quad . \tag{12}$$

Where, the average heat transfer rate, $\dot{\bar{Q}}_{cyl,wall}$, is calculated by integrating the instantaneous heat transfer between the in-cylinder refrigerant gas and cylinder wall over one second.

The heat transfer rates, $\dot{Q}_{plate,gas}$, $\dot{Q}_{gas,shell}$, $\dot{Q}_{shell,amb}$, $\dot{Q}_{plate,amb,1}$, $\dot{Q}_{plate,amb,2}$, $\dot{Q}_{pipe,amb}$ can be expressed using the following general form,

$$\dot{Q}=\frac{T_a-T_b}{R_{ab}}. \tag{13}$$

Where, T_a-T_b is the temperature difference between two components. R_{ab} is the heat transfer thermal resistance. In order to find the thermal resistance, empirically correlated averaged Nusselt numbers are determined first considering different types of free convections shown in Figure 2. Since the ambient air and refrigerant gas inside the shell are both assumed to be quiescent, all heat transfer between the ambient air/refrigerant gas and compressor components are free convection.

3. NUMERICAL METHODOLOGY

The classical 4th-order Runge-Kutta method is used to solve the initial value problem formed by the combination of Eq. (3) and Eq. (4). As it is known, once the initial state of in-cylinder refrigerant together with other required information (such as initial suction/discharge valve plate positions) are given, the compression process model can be solved. The final in-cylinder refrigerant state and suction/discharge valve plate positions after one driving shaft rotation should match the initial values. However, since the initial values are arbitrarily assumed, it is not guaranteed that the final values would match the initial values. In this case, the problem becomes a root-finding problem for the following equation,

$$\vec{x} - g(\vec{x}) = 0. \tag{14}$$

Where $\vec{x}$ is a vector comprised of the parameters whose values are initially required to carry out the solution of the compression process model and g is a function of period of 2π. The root of the above equation is the initial values which would match the final values. Therefore, the Broyden's method is employed here (Bradie, 2006).

The cylinder wall temperature and the temperature of the refrigerant gas inside the shell are required to solve the compression process model. However, since the actual values of these two temperatures are unknown initially, arbitrary values are chosen. In order to get the actual cylinder wall temperature and refrigerant gas temperature inside the shell, the compressor overall energy balance model is incorporated with the compression process model. The bottom dead center (B.D.C.) is chosen as the starting point of the piston.

The converging criterion for the overall energy balance model is 10^{-4}. The converging criterion to find the initial values in the compression process model is also 10^{-4}. The flow chart of the algorithm is given in Figure 3.

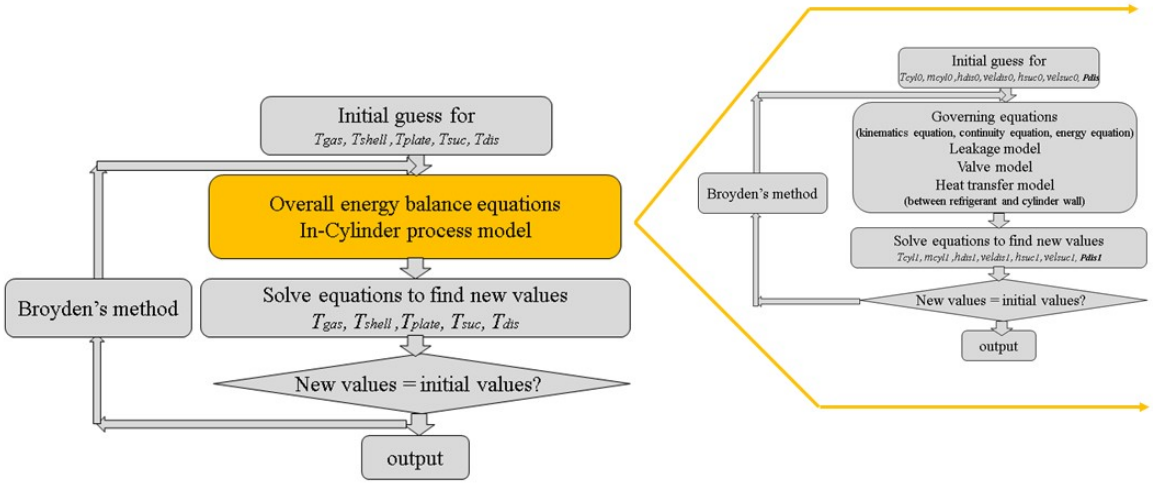

Figure 3: The algorithm flow chart of the whole compressor model

4. RESULTS AND DISCUSSION

4.1 Kinematics model

A prototype five-piston axial reciprocating compressor using the S-RAM mechanism was simulated using a suction pressure of 26 bars, discharge pressure of 90 bars, and rotational speed of 900 rpm. The variations of piston displacement, velocity and acceleration with respect to the machine driving shaft rotational angle are shown in Figure 4. It is clearly shown that all pistons in the five cylinders are moving similarly except for the phase difference. The piston starting point is located at the B.D.C.

Figure 5 provides the moving path of a ball center, which is clearly seen not to be located on the cylinder centerline leading to a side load to the restraints. The center of ball is moving with a 'figure 8' motion. The red vertical line is the centerline of one of the cylinders.

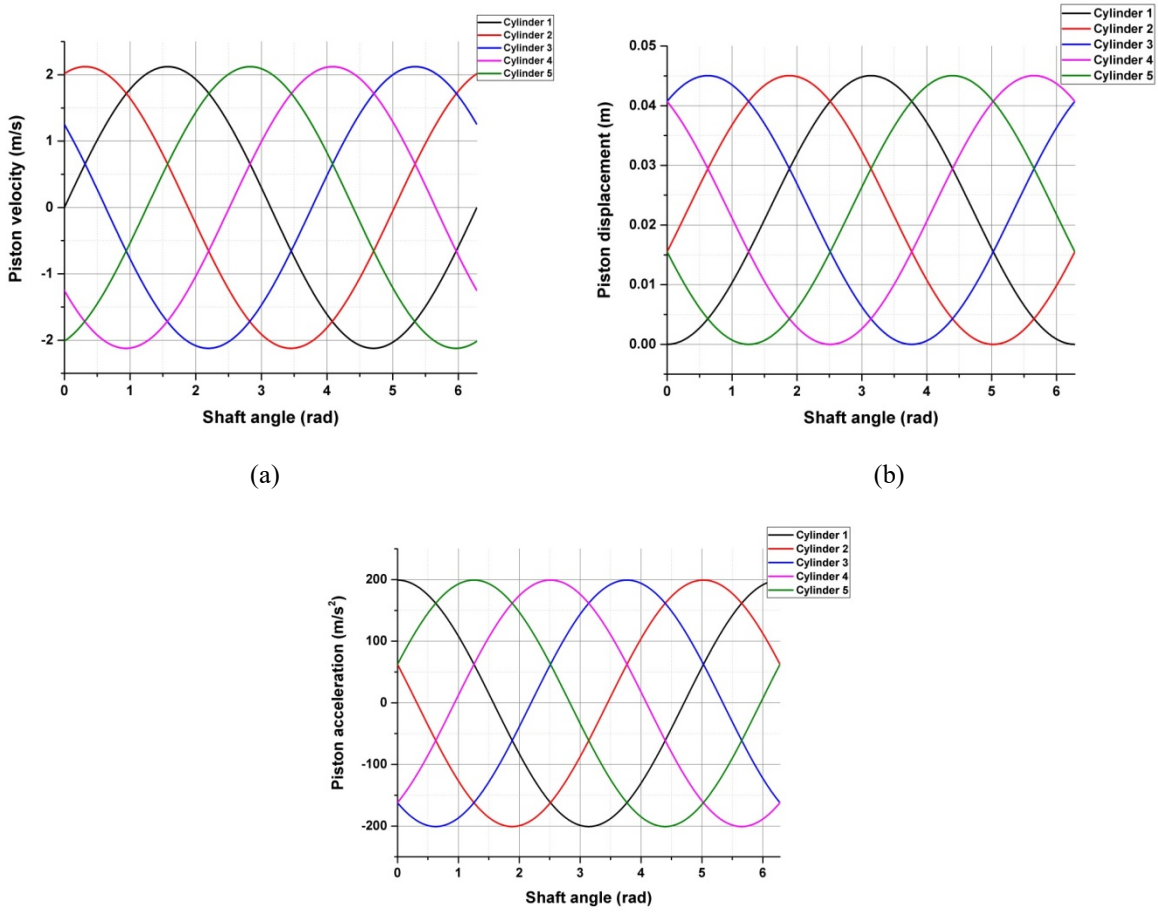

Figure 4: Piston displacement, velocity and acceleration (stroke = 0.04445 m) versus driving shaft angle (a) displacement; (b) velocity; (c) acceleration

4.2 Compression Process Model

The indicated P-V diagram for the prototype compressor is given in Figure 6. In the discharge process, the in-cylinder pressure reaches a value that is at first higher than the pressure in the discharge pipeline to overcome the valve spring force before the valve opens. As the discharge valve opens, some amount of refrigerant flows out of the cylinder decreasing the pressure inside the cylinder. The discharge valve starts to close when the in-cylinder pressure is not high enough to hold the resultant force of the valve spring and the discharge pressure behind valve. Hence, the discharge valve moves back and forth during the discharge process as shown in Figure 7.

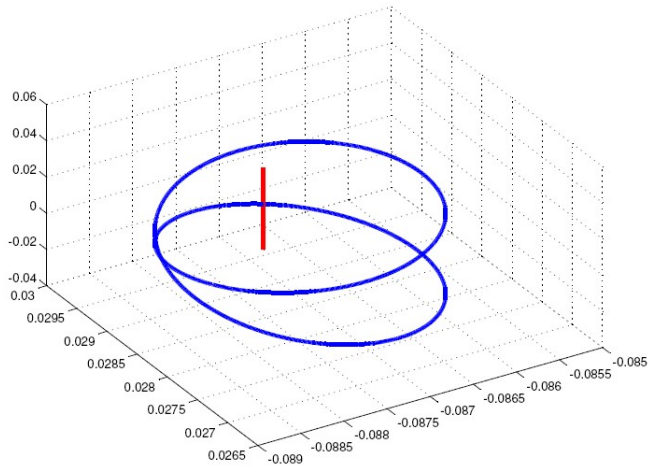

Figure 5: Moving path of a ball center ('figure 8' motion)

Figure 7 shows the variation of suction/discharge valve plate displacement with respect to the compressor driving shaft rotational angle. It can be seen that the suction valve is still open when the compression process starts. The discharge valve also stays open when the re-expansion process begins. Back flow may occur for both suction and discharge valves due to the late closing of the valve plates. The closing time of the valve plate can be adjusted by optimizing the valve spring stiffness and valve lift.

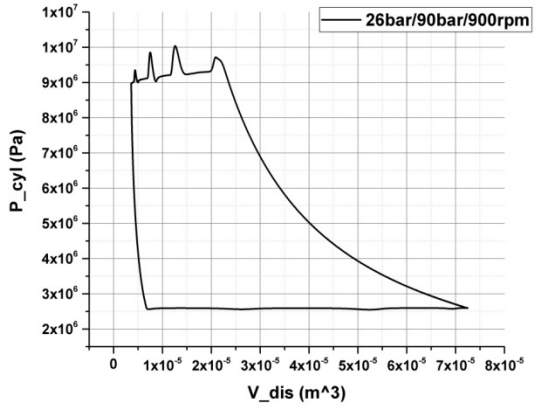

Figure 6: In-cylinder refrigerant pressure versus piston displacement volume

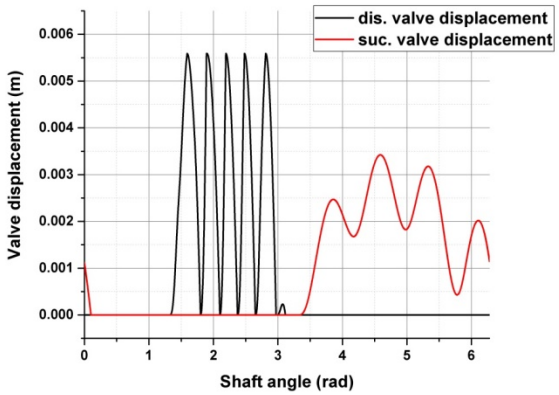

Figure 7: Valve displacement (26bar/42bar, 900 rpm)

4.3 Parametric Studies

4.3.1 Effect of Discharge Pressure

The effect of discharge pressure on the P-V diagram is shown in Figure 8. The suction pressure stays constant. As it is shown, the duration of the re-expansion process for a higher discharge pressure case is longer than that for a lower discharge pressure case. This is one of the reasons accounting for the decrease of the volumetric efficiency with an increment in pressure ratio, since less volume is available for the suction gas through the suction valve if a higher discharge pressure is applied. The discharge valve starts to open earlier for the low discharge pressure. Moreover, the in-cylinder pressure fluctuation is smoother for the higher discharge pressure case, which is consistent with the discharge valve movement shown in Figure 9.

Figure 10 shows the variation of the instantaneous heat transfer between in-cylinder refrigerant gas and cylinder wall with respect to the machine driving shaft angle. The shapes of the curves for both low and high pressure ratio

cases are similar except that the magnitude of the heat transfer rate is larger for high pressure ratio case since the in-cylinder refrigerant temperature is higher, which can be seen in Figure 11. The trend of these two curves agrees well with that discovered by Recktenwald (1989).

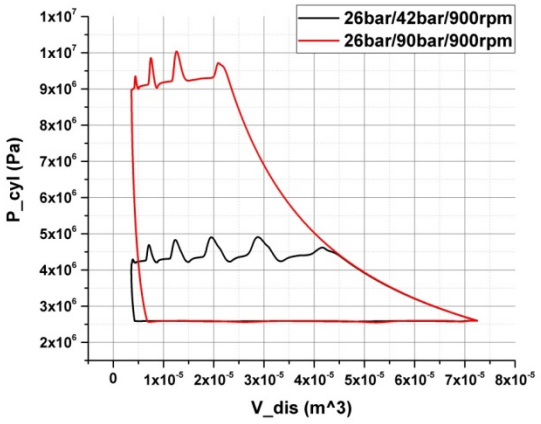

Figure 8: Effect of discharge pressure on P-V diagram

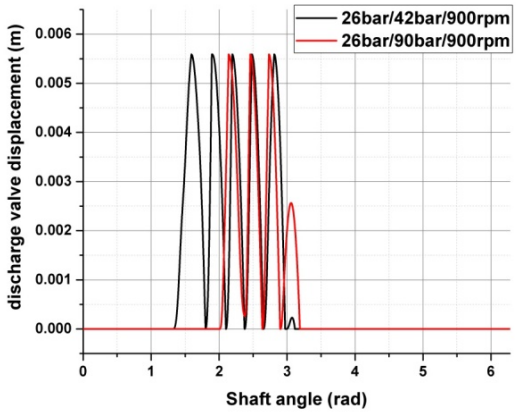

Figure 9: Effect of discharge pressure on discharge valve displacement

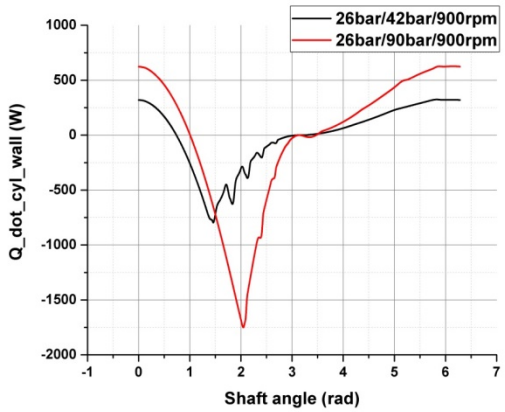

Figure 10: Effect of discharge pressure on the instantaneous heat transfer between in-cylinder refrigerant and cylinder wall

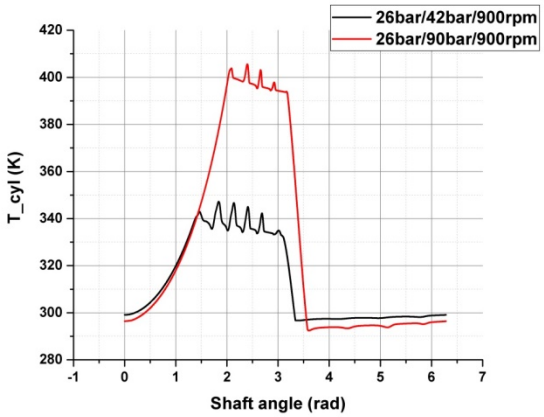

Figure 11: Effect of discharge pressure on the in-cylinder refrigerant temperature

4.3.2 Effect of Stroke-to-Bore Ratio

The stroke-to-bore ratio is an important parameter, which has a great influence on the reciprocating compressor performance. Figure 12 shows the variation of instantaneous leakage mass flow rate leaving from the in-cylinder control volume with respect to the stroke-to-bore ratio. It should be noted that the results presented in Figure 12 and Figure 13 are determined with the assumption that the compressor stroke is kept constant while the cylinder bore diameter is changing. It is clearly shown that the magnitude of the instantaneous leakage mass flow rate increases with the stroke-to-bore ratio decreases. A reduced stroke-to-bore ratio leads to a larger cylinder bore diameter when the stroke is constant. The leakage path is increased with a large cylinder bore diameter causing more leakage.

The effect of stroke-to-bore ratio on the instantaneous heat transfer rate between in-cylinder refrigerant and cylinder wall is given in Figure 13. It is found that the magnitude of the heat transfer rate has a higher value with a lower stroke-to-bore ratio. The heat transfer surface area is enlarged with a smaller stroke-to-bore ratio since the cylinder bore diameter is increased, causing the increment of the heat transfer rate.

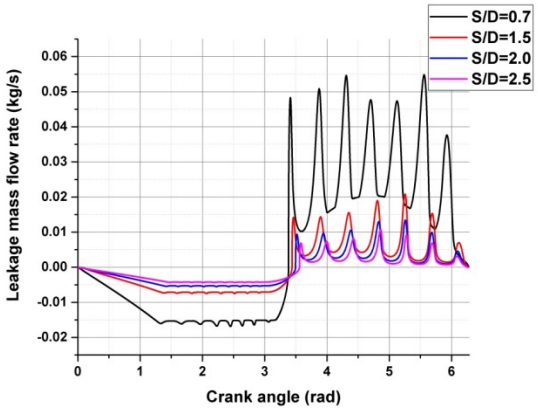

Figure 12: Effect of stroke-to-bore ratio on the instantaneous leakage mass flow rate (26bar/42bar/600rpm)

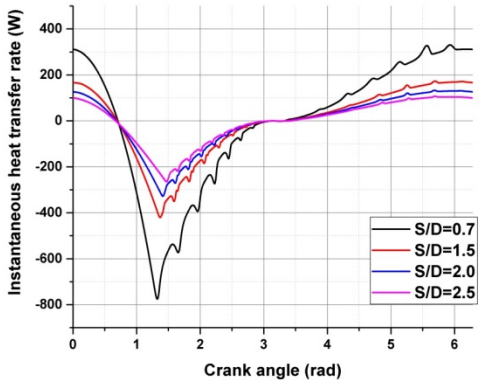

Figure 13: Effect of stroke-to-bore ratio on the instantaneous heat transfer rate between in-cylinder refrigerant and cylinder wall (26bar/42bar/600rpm)

5. CONCLUSIONS AND FUTURE WORK

A comprehensive simulation model to predict the performance of a prototype reciprocating compressor using the S-RAM mechanism is introduced. The comprehensive model is comprised of a kinematics model, compression process model and an overall energy balance model. In the kinematics model, the movement of the piston is revealed. The in-cylinder refrigerant pressure and temperature are given by solving the compression process model incorporated with kinematics model. The values of cylinder wall temperature, suction and discharge temperatures in their connection pipes are provided from the overall energy balance model. The gas pulsation issue in the discharge pipes is also considered. Parametric studies are conducted to investigate the effects of discharge pressure and stroke-to-bore ratio. It is shown that the stroke-to-bore ratio is critical for the compressor design to improve the volumetric efficiency by controlling the leakage through the leakage path between piston and cylinder wall.

It should be noted here that the dynamics model is not included in the current model, which is the focus of the future work. Therefore, currently only a certain portion of indicated power is assumed to be the frictional power loss.

NOMENCLATURE

A	area	h	unit enthalpy, distance between driving shaft center-line and cylinder centerline, heat transfer coefficient
C	discharge coefficient , specific heat capacity	m	mass
D	diameter	p	pressure
L	Length	ν	specific volume
Q	quantity of heat transferred to control volume through boundary from its ambient	x	piston displacement
R	Length, or heat transfer thermal resistance	α	angle
S	piston stroke	θ	angle
T	temperature	κ	specific heat ratio
U	mean velocity of piston	μ	dynamic viscosity
W	work	ρ	density
Z	compact factor of carbon dioxide, or acoustic impedance at the discharge valve	τ	thermal conductivity of refrigerant in control volume
g	function	ω	angular speed of the main crankshaft

Subscript

0	clearance volume
amb	ambient
c	refrigerant in control volume
comp	compressor
cyl	cylinder
D	drag coefficient
d	Downstream
dis	Discharge
f	film
gap	leakage gap
heat	heat transfer
high	high pressure side
imp	impedence
li, lo	leak in and out
low	low pressure side
mean	mean velocity of piston
p	piston
plate	cylinder plate
port	valve port
pul	gas pulsation
s	surface
shaft	crank shaft
suc	suction
u	upstream
valve	valve
vp	valve plate
w	wobble plate
wall	cylinder wall
∞	ambient

REFERENCES

Adair R P, Qvale E R, Pearson J T 1972. Instantaneous heat transfer to the cylinder wall in reciprocating compressors. Proc. of the Int. Comp. Eng. Conf. Purdue University, West Lafayette, IN USA, pp. 521-526.

Brablik J 1972. Gas pulsations as factor affecting operation of automatic valves in reciprocating compressors. Proc. of the Int. Comp. Eng. Conf. Purdue University, West Lafayette, IN USA.

Bradie B 2006. A friendly introduction to numerical analysis. Peason Prentice Hall, USA.

Baumannn H, Conzett M 2002. Small oil free piston type compressor for CO2. Proc. of the Int. Comp. Eng. Conf. Purdue University, West Lafayette, IN USA, pp. 861-868.

Cavalcante P, Försterling S, Tegethoff W, Stulgies N, Köhler J 2008. Transient Modeling and Sensitivity Analysis of a Controlled R744 Swash Plate Compressor. Proc. of the Int. Comp. Eng. Conf. Purdue University, West Lafayette, IN USA, paper 1880.

Elson J P, Soedel W 1974. Simulation of the interaction of compressor valves with acoustic back pressures in long discharge lines. J. Sound Vib 34 (2), pp. 211-220.

Fagerli B 1997. CO2 compressor development IEA/IIR Workshop on CO2 Technologies in Refrigeration, Heat Pump and Air Conditioning Systems: Trondheim, pp. 13-14.

Furuhama S, Tada T 1961. On the flow of the gas through the piston-rings (1st report, the discharge coefficient and temperature of leakage gas). Bulletin of JSME 4 (16), pp. 684-690.

Kim J H, Groll E A 2007. Feasibility study of a bowtie compressor with novel capacity modulation. Int. J. Refrigeration 30, pp. 1427-1438.

Lemmon, E. and Huber, M., Refprop 7.0, 2012, http://www.nist.gov/srd/nist23.htm

Lin M, Sun S Y 2006. Theory of the piston compressor. Xi'an Jiaotong University Press. Xi'an, China.

Lorentzen G, Pettersen J 1992. New possibilities for non-CFC refrigeration. IIR International Symposium on Refrigeration, Energy and Environment: Trondheim, pp. 147-63.

Nekså P, Rekstad H, Zakeri G, Schiefloe, P A 1999. Commercial heat pumps for water heating and heat recovery. IEA/IZWe.V./IIR Workshop on CO2 Technology in Refrigeration, Heat Pump and Air Conditioning System: Mainz.

Officine Mario Dorin. http://www.dorin.com/jsp/Template2/HomePage.jsp.

Recktenwald G W 1989. A study of heat transfer between the walls and gas inside the cylinder of a reciprocating compressor. PhD. Thesis. University of Minnesota. pp. 197-199.

Süss J, Kruse H 1998. Efficiency of the indicated process of CO2 compressors. International Journal of Refrigeration, 21(3), pp. 194-205.

Todescat M L, Fagotti F, Prata A T, Ferreira R T S 1992. Thermal energy analysis in reciprocating hermetic compressors. Proc. of the Int. Comp. Eng. Conf. Purdue University, West Lafayette, IN USA, pp. 1419-1428.

Yang B, Bradshaw C, Groll E A 2013. Modeling of a semi-hermetic CO2 reciprocating compressor including lubrication submodels for piston rings and bearings. Int J. Refrigeration 36 (7), pp.1925-1937.

ACKNOWLEDGEMENT

The authors would like to thank S-RAM Dynamics Inc. for the support to conduct this study.